

The Energy Spectrum of Stochastic Eddies with Gamma Distribution

Rukiye Kara^{1,*} and Mine Çağlar²

¹ Department of Mathematics, Mimar Sinan Fine Arts University, Istanbul, Turkey

² Department of Mathematics, Koç University, Istanbul, Turkey

Received: 6 Nov. 2013, Revised: 7 Mar. 2014, Accepted: 8 Mar. 2014

Published online: 1 Feb. 2015

Abstract: Çinlar velocity field which is based on eddies of rotational form is a promising subgrid velocity model for its use in large eddy simulation (LES). This has been confirmed by data analysis of high frequency radar observations. The energy spectrum plays a central role for representing the subgrid scales in filtered Navier-Stokes equations used in LES. We consider a truncated Gamma distribution for eddy sizes to replicate the subgrid scale energy spectrum analytically. Kolmogorov proposed a form of the spectrum that extends to the inertial scale. Lundgren vortex has a spectrum involving an exponential function and has been used in LES. Çinlar velocity spectrum which is based on the truncated Gamma distribution indicates a good match with the spectrum estimated from real data. The results of this study can be used for designing a method for representing the small scale structures in LES by modeling the subgrid stress.

Keywords: Stochastic flows, Kolmogorov spectrum, homogeneous turbulence, subgrid model

1 Introduction

The turbulence theory examines continuous change of eddy sizes. The largest eddies break down to the smaller eddies which further break down to even smaller ones. This process is defined as the kinetic energy transfer from the large-scale flow to the smaller. The turbulent flow is determined by Navier-Stokes equations. However, exact solution of these equations is still impossible. The most precise approach to solve the full Navier-Stokes equations is direct numerical simulation (DNS), which requires to represent all the scales from the smallest to the largest. Clearly, this is expensive in time and computer capacity. An efficient approach is large eddy simulation (LES) based on numerical solution of larger eddies while only modeling the smaller ones. In LES, a filtering operation is used to separate the large scales (low frequency) from small scales (high frequency). Then, the subgrid stress which remains unresolved is modeled by various approaches.

LES has been introduced by Smagorinsky [42] firstly for simulating atmospheric and oceanic models. Based on Boussinesq hypothesis for energy transfer and turbulence proposed by Richardson [38] and Kolmogorov [24] to subgrid modeling, Smagorinsky's subgrid model was the

first to use eddy viscosity for subgrid stress. Lilly [29,30] and Deardorff [18] were among the first to further develop and use the LES models. Leonard [27] introduced the filter function form used today. In 1970's Kraichnan [26] developed an eddy viscosity concept for spectral space. Bardina et al. [3] developed scale similarity model which is based on the assumption that structure of the smallest resolved scales is similar to structure of the largest unresolved scales. In 1991, Germano, Piomelli, Moin and Cabot [22] introduced dynamic eddy viscosity model in which the eddy viscosity coefficient is computed dynamically. Domaradzki and Saiki [19] focused on the estimation of the unresolved velocity field for LES. Several variations of these subgrid scale models have also been proposed [34,40].

Different from the above models, Misra and Pullin [35] developed a subgrid model based on stretched vortices. The orientation of the vortices is determined by the resolved scales and randomized parameters. The origin of this model is the study of Lundgren [31] where it has been shown that the energy spectrum of spiral vortex structures includes an exponential function as well as the scaling $k^{-5/3}$. In 1941, Kolmogorov [24] proposed the asymptotic form of energy spectrum of

* Corresponding author e-mail: rukiye.kara@msgsu.edu.tr

incompressible turbulent flow as

$$\mathcal{E}(|k|) = \varepsilon^{2/3} |k|^{-5/3} F(\eta|k|) \quad (1)$$

for large wavenumbers k where ε is dissipation rate per unit mass, η is called Kolmogorov length with $\eta = (\nu^3/\varepsilon)^{1/4}$ and ν is viscosity. In the inertial range, this should reduce to the form $\mathcal{E}(|k|) = C\varepsilon^{2/3}|k|^{-5/3}$ where C is a constant. Townsend [44], Corrsin [17], Tennekes [43] and Saffman [39] have revealed specific models of fine-scale structure. Burger has given stretched vortex solutions of the 3D Navier-Stokes (and Euler) equations, and Townsend [44] has used this solution in the turbulence application based on a random collection of vortex tubes and vortex sheets. The stretched spiral vortex solution for fine scale structure proposed by Lundgren [31] is based on Burgers' vortices and Townsend collection. The resulting energy spectrum of small scale structure is given by

$$\mathcal{E}(|k|) = C\varepsilon^{2/3}|k|^{-5/3} \exp\left[\frac{-2\nu}{3a}|k|^2\right] \quad (2)$$

where C is a universal constant and a is the strain rate. Chung [13] has first used Lundgren energy spectrum for the stretched-vortex subgrid stress model.

In this paper, our aim is to derive the small scale energy spectrum of Çınlar velocity field which is also based on vortex structures. It has been studied in a series of papers [6, 7, 8, 9, 10, 11] as a model for small to medium scale turbulent flow. In Çağlar [9], Çınlar velocity field is validated with high frequency radar data. Its parameters have been statistically estimated and it has been shown to represent the Eulerian dynamics in approximately an 11kmx11km area very well. This scale would correspond roughly to a single grid in LES and would remain unresolved if not modeled. Therefore, Çınlar velocity has been put forward as a promising subgrid velocity field. The compliance with the Kolmogorov $-5/3$ rule of the energy spectrum of Çınlar velocity field has also been investigated for the inertial range [10].

The results of the present work are useful for designing a subgrid algorithm for LES based on the energy spectrum, which is used to approximate the subgrid stress. The ultimate aim is to link the parameters of the spectrum to the resolved scales in order to solve the filtered equations of motion. It can be argued that consideration of only a second order quantity such as the spectrum makes the result indistinguishable from a Gaussian velocity field. However, the subgrid stress also involves the covariance of the resolved velocity with the subgrid velocity. Using a subgrid velocity consistent with real data makes a difference at this stage. Çınlar velocity model originates from observed structures of eddies and randomness in the ocean at small scales. In particular, the statistics of velocity increments and velocity gradients indicate that small scale turbulence is highly non-Gaussian [20, Sec.8], [28]. With a Gaussian velocity

field, the third moment of the velocity increments would vanish, contradicting with the 4/5 law proved by Kolmogorov [20]. Çınlar velocity captures negative skewness predicted by this law. Let the velocity increment be defined by $\delta u_{||} = (u(x+r) - u(x)) \cdot \frac{r}{|r|}$. The third order structure function of Çınlar velocity field is found as

$$\mathbb{E}(\delta u_{||}^3) = \frac{\lambda \mathbb{E}(a^3)}{c\Gamma_{B/\zeta}(\theta)\zeta^\theta} \int_{\mathbb{R}^2} \int_0^B dz db b^{\theta-1} e^{-b/\zeta} \cdot \left[\left(\frac{z_1 r_2 - z_2 r_1}{|r|} \right) \left(\frac{m(|(z+r)/b|)}{|z+r|} - \frac{m(|z/b|)}{|z|} \right) \right]^3$$

the derivation of which is given in Appendix. For this expression to be negative, the distribution of a can be chosen negatively skewed so that $\mathbb{E}(a^3)$ is negative. This follows because the integral turns out to be positive except for very small values of r corresponding to much smaller scales than the inertial range.

We investigate the energy spectrum for small scale structures by using a Gamma distribution for eddy radius. Since Gamma density has both a power term and an exponential term, it is considered as a comparable choice for generating an energy spectrum with exponential function as in (2) for Lundgren vortex. In fact, a widely proposed form for $\mathcal{E}(|k|)$ is

$$\mathcal{E}(|k|) \sim (|k|\eta)^\alpha \exp(-\beta(|k|\eta)^n) \quad (3)$$

in the dissipation range [33]. The power of $|k|$ is not necessarily $-5/3$ in (3) since the spectrum may not have an inertial range as in Burger's vortex tube which has a spectrum $\sim |k|^{-1} \exp(-\beta(|k|\eta)^2)$ [31]. We show that our energy spectrum has a similar form to (1) as suggested by Kolmogorov while the function F remains implicit as

$$\mathcal{E}(|k|) \sim |k|^{-\theta-4} F(B|k|)$$

where $\theta > 0$ is the shape parameter of the Gamma distribution and B plays the role of Kolmogorov length scale. Since F remains unspecified, the power of $|k|$ is not necessarily $-5/3$. Therefore, we use the spectrum of real subgrid velocity data for a numeric fit of F . As a result, a Gamma distribution for eddy sizes is validated due to a close fit in the wavenumber space. More precisely, a truncated Gamma distribution is used for the subgrid scale under consideration. The parameters of the distribution are estimated directly from the radius data.

There has been considerable debate about the values of the parameters α , β and n of (3) in the literature. The energy spectrum with respect to n has been examined by many scientists. Townsend [44] and Novikov [36] suggested $n = 2$ at scales much smaller than η , the dissipation length scale [33]. There are only few studies for determining α and β . Most models suggest $\alpha = -5/3$ for lower wavenumber because of its consistency with Kolmogorov's scaling. On the other hand, Kraichnan [25] and Orszag [37] have predicted $\alpha = 3$. As a result of numerical studies, Kida et al. [23] found that $\alpha < 0$. Kida

et al. argue that the negative value for α is connected to energy transfer in the dissipation range. In particular, Martinez et al. [33] have investigated the possible values of α and β for high frequency depending on $|k|\eta$ by high-resolution, direct numerical simulations of three-dimensional incompressible Navier-Stokes equations. It has been found that β is fairly constant at a value between 5 and 6, except for $|k|\eta \approx 4$. When $|k|\eta \approx 4$, β drops to about 4. For α , all results obtained from the range $|k|\eta < 3$ are consistently negative, within the range -1 to -2 . Near the range $|k|\eta \approx 4$, α drops to about -6 , then increases to positive values and remains fairly constant at a value between 4 and 6 when $8 < |k|\eta < 10$.

The paper is organized as follows. In Section 2, a review of Çinlar velocity field is given. In Section 3, the energy spectrum of the fine scales is derived using a truncated Gamma distribution. Real subgrid scale velocity data are studied to validate the Gamma model in Section 4. Finally, the conclusions are given in Section 5.

2 Subgrid Velocity Model

In this section, we review flows generated by Çinlar velocity fields. The velocity field is composed of eddies randomized through their types and arrival times. They decay exponentially in time to form a stationary, Markovian velocity field. The motivation comes from vortex development and decay observed in the ocean [41]. The flow is incompressible and isotropic due to the form of the eddies. In contrast to Brownian flows where the Eulerian velocity is delta-correlated, Çinlar velocity field itself is Markovian, which implies medium to long-term correlated flows. In this paper, we consider the generalized form in [10] where the decay rate of each eddy depends on its type.

Let v be a deterministic velocity field on \mathbb{R}^2 called the basic eddy, and let $Q = \mathbb{R}^2 \times \mathbb{R} \times (0, \infty)$ be an index set. Eddies of different sizes and amplitudes for $q \in Q, x \in \mathbb{R}^2$ are obtained by

$$v_q(x) = av \left(\frac{x-z}{b} \right), \quad q = (z, a, b)$$

where q represents the type of an eddy and includes its center z in space, its amplitude a as well as its radius b . Let N be a Poisson random measure on the Borel sets of $\mathbb{R} \times Q$ with mean measure

$$\mu(dt, dq) \equiv \mu(dt, dz, da, db) = \lambda dt dz \alpha(da) \beta(db)$$

where λ is the arrival rate per unit time-unit space, and α and β are probability distributions. The arrival (appearance) time t of an eddy, its center, amplitude and radius are all randomized with N . By the superposition of these eddies decaying exponentially in time with rate

$$c_q(x) = c \left| \frac{x-z}{b} \right|^{2\gamma}$$

for $q = (z, a, b)$ and constant $c > 0$, a stationary velocity field u is constructed as

$$u(x, t) = \int_{-\infty}^t \int_Q N(ds, dz, da, db) \cdot \exp(-c|(x-z)/b|^{2\gamma}(t-s)) av \left(\frac{x-z}{b} \right)$$

where $x \in \mathbb{R}^2, t \in \mathbb{R}, c > 0, \gamma > 0$, as the generalized form of Çinlar velocity field [10].

We consider an incompressible and isotropic flow in \mathbb{R}^2 . Therefore, the basic eddy $v = (v_1, v_2)$ is taken as a rotation around 0 with magnitude $m(r)$ at distance r from 0, where $m: \mathbb{R} \rightarrow \mathbb{R}_+$ is continuous and has support $[0, 1]$. For example, $m(r)$ can be taken as $m(r) = (1 - \cos 2\pi r)/2, 0 \leq r \leq 1$, and $m(r) = 0$ otherwise, as in [6]. The specific equations for v are

$$v_1(x) = -\frac{x_2}{r} m(r), \quad v_2(x) = \frac{x_1}{r} m(r)$$

where $x = (x_1, x_2)$ and $r = |x| \in [0, 1]$. Then, every eddy is a rotation, since it is translation, amplification and dilation of v . Although this form of Çinlar velocity field on \mathbb{R}^2 has been extensively studied, it can be extended to \mathbb{R}^3 when the basic eddy is chosen in three dimensions. A simple choice would be to take the support of the basic eddy as the unit sphere in \mathbb{R}^3 , in analogy with the unit disk used in two dimensions, where the planar motion can be taken as a rotation.

The correlation tensor of the velocity field is computed as

$$R_{ij}(x, t) = \frac{\lambda}{c} \int_{\mathbb{R}^2} dz \int_{\mathbb{R}} \alpha(da) a^2 \cdot \int_{\mathbb{R}_+} \beta(db) \frac{b^2 \exp(-c|z|^{2\gamma}|t|)}{|z|^{2\gamma} + |z + \frac{x}{b}|^{2\gamma}} v_i(z) v_j \left(z + \frac{x}{b} \right) \tag{4}$$

for $x \in \mathbb{R}^2$ and $t \in \mathbb{R}$, where the time integral has already been taken. In [10], a piecewise Pareto distribution is chosen for the eddy radius as

$$\beta(db) = \begin{cases} \delta l_1^\delta b^{-\delta-1} db & \text{if } l_1 \leq b \leq l_2 \\ \theta l_1^\delta l_2^{\theta-\delta} b^{-\theta-1} db & \text{if } b \geq l_2 \end{cases}$$

where $\delta, \theta > 0$ are the parameters to capture power-law dependence, and $l_1, l_2 > 0$ serve as the cutoff scales. Then, the energy spectrum is obtained as

$$\mathcal{E}(|k|) = \frac{\lambda \delta l_1^\delta \mathbb{E}a^2}{4\pi c} |k|^{\delta-3} \int_{|k|l_1}^{|k|l_2} db b^{3-\delta} f(b) + \frac{\lambda \theta l_1^\delta l_2^{\theta-\delta} \mathbb{E}a^2}{4\pi c} |k|^{\theta-3} \int_{|k|l_2}^\infty db b^{3-\theta} f(b)$$

where

$$f(b|k|) := \sum_{j=1}^2 \int_{\mathbb{R}^2} dz e^{ibk \cdot z} v_j(z) \int_{\mathbb{R}^2} dx e^{-ibk \cdot x} \frac{v_j(x)}{|z|^{2\gamma} + |x|^{2\gamma}}$$

and is compatible with Kolmogorov $-5/3$ rule in the inertial range with $\delta = 4/3$ and $\gamma = 1/3$.

In this paper, we choose the distribution β of b as a right-truncated Gamma distribution [21] given by

$$\beta(db) = \frac{b^{\theta-1} \exp(-b/\zeta)}{\Gamma_{B/\zeta}(\theta) \zeta^\theta} db, \quad 0 < b < B \quad (5)$$

where $\theta > 0$ and $\zeta > 0$ are the shape and scale parameters, respectively, and $\Gamma_{B/\zeta}(\theta)$ is the incomplete Gamma function with parameter θ and integration bounds from 0 to B/ζ . It follows that only small scale eddies up to some cutoff B are considered. Gamma distribution, which involves an exponential term in contrast to Pareto, is used for the purpose of capturing an energy spectrum of the form (1) possibly involving an exponential term like the vortex tube and Lundgren vortex. Moreover, a truncated Gamma distribution is indicated by an analysis of real data in [9, Fig.6]. We now substitute (5) in (4) to get

$$R_{ij}(x, t) = \frac{\lambda}{c\Gamma_{B/\zeta}(\theta) \zeta^\theta} \int_{\mathbb{R}} \alpha(da) a^2 \int_{\mathbb{R}^2} dz \exp(-c|z|^{2\gamma}|t|) \cdot \int_0^B db b^{\theta+1} \exp(-b/\zeta) \frac{v_i(z) v_j(z + \frac{x}{b\zeta})}{|z|^{2\gamma} + |z + \frac{x}{b\zeta}|^{2\gamma}}. \quad (6)$$

3 The Energy Spectrum

The Fourier transform E of R is called the spectral density tensor given by

$$E_{ij}(k, \omega) = \frac{1}{(2\pi)^2} \int_{\mathbb{R}} \int_{\mathbb{R}^2} \exp(-\mathbf{i}(k \cdot x + \omega t)) R_{ij}(x, t) dx dt.$$

Turbulent energy per unit mass is defined by

$$\frac{1}{2} \int_{\mathbb{R}^2} (E_{11} + E_{22}) dk = \frac{1}{2} \int_{\mathbb{R}^2} \sum_{j=1}^2 \frac{1}{4\pi^2} \cdot \int_{\mathbb{R}^2} \exp(-\mathbf{i}k \cdot x) R_{jj}(x, 0) dx dk$$

and is equivalent to

$$\frac{1}{2} \int_{\mathbb{R}^2} \sum_{j=1}^2 \frac{1}{4\pi^2} \int_{\mathbb{R}^2} \exp(-\mathbf{i}k \cdot x) R_{jj}(x, 0) dx dk =: \int_0^\infty \mathcal{E}(|k|) d|k|$$

where $\mathcal{E}(|k|)$ is the energy spectrum and a function of only $|k|$ due to isotropy.

We use the truncated Gamma distribution (5) to find the form of the turbulent energy spectrum. By putting $b' =$

b/ζ , we get

$$\int_{\mathbb{R}^2} \exp(-\mathbf{i}k \cdot x) R_{jj}(x, 0) dx = \frac{\lambda \mathbb{E}(a^2) \zeta^2}{c\Gamma_{B/\zeta}(\theta)} \int_{\mathbb{R}^2} dz v_j(z) \cdot \int_0^{B/\zeta} db b^{\theta+1} \exp(-b) \int_{\mathbb{R}^2} dx \frac{\exp(-\mathbf{i}k \cdot x) v_j(z + \frac{x}{b\zeta})}{|z|^{2\gamma} + |z + \frac{x}{b\zeta}|^{2\gamma}}$$

from (6). By rearranging the integrals and making a change of variable $x' = z + \frac{x}{b\zeta}$, we find

$$\int_{\mathbb{R}^2} \exp(-\mathbf{i}k \cdot x) R_{jj}(x, 0) dx = \frac{\lambda \mathbb{E}(a^2) \zeta^4}{c\Gamma_{B/\zeta}(\theta)} \cdot \int_{\mathbb{R}^2} dz \exp(\mathbf{i}b\zeta k \cdot z) v_j(z) \int_0^{B/\zeta} db b^{\theta+3} \exp(-b) \cdot \int_{\mathbb{R}^2} dx \frac{\exp(-\mathbf{i}b\zeta k \cdot x) v_j(x)}{|z|^{2\gamma} + |x|^{2\gamma}}.$$

Then, we get the energy spectrum as

$$\mathcal{E}(|k|) = \frac{\lambda \mathbb{E}(a^2) \zeta^4}{8\pi^2 c\Gamma_{B/\zeta}(\theta)} \int_0^{B/\zeta} db b^{\theta+3} \exp(-b) \cdot \int_{\mathbb{R}^2} dz \exp(\mathbf{i}b\zeta k \cdot z) \cdot \int_{\mathbb{R}^2} dx \frac{\exp(-\mathbf{i}b\zeta k \cdot x) (v_1(x) v_1(z) + v_2(x) v_2(z))}{|z|^{2\gamma} + |x|^{2\gamma}}.$$

In the rest of this section, we derive the asymptotical form of the energy spectrum \mathcal{E} for large $|k|$, as large $|k|$ values correspond to subgrid scales. We first do a radial transform as follows

$$k = (k_1, k_2) = (|k| \cos \alpha, |k| \sin \alpha) \quad (7)$$

$$x = (x_1, x_2) = (|x| \cos \varphi, |x| \sin \varphi)$$

$$z = (z_1, z_2) = (|z| \cos \psi, |z| \sin \psi)$$

to obtain

$$\mathcal{E}(|k|) = \sum_{j=1}^2 \frac{\lambda \mathbb{E}(a^2) \zeta^4}{8\pi^2 c\Gamma_{B/\zeta}(\theta)} \int_0^{B/\zeta} e^{-b} b^{\theta+3} db \cdot \int_0^{2\pi} d\psi \int_0^1 d|z| \int_0^{2\pi} d\varphi \cdot \int_0^1 d|x| \exp(\mathbf{i}\zeta b |k| |z| \cos(\psi - \alpha)) |z| v_j(|z|, \psi) \cdot \exp(-\mathbf{i}\zeta b |k| |x| \cos(\varphi - \alpha)) |x| \frac{v_j(|x|, \varphi)}{|x|^{2\gamma} + |z|^{2\gamma}}.$$

The following expansion of the exponential function with Bessel functions will be useful. We have

$$\exp(\mathbf{i}z \cos(\theta)) = \sum_{n=-\infty}^{\infty} \mathbf{i}^n J_n(z) \exp(\mathbf{i}n\theta) = \sum_{n=0}^{\infty} J_n(z) [\mathbf{i}^n \exp(\mathbf{i}n\theta) + (-1)^n \mathbf{i}^{-n} \exp(-\mathbf{i}n\theta)]$$

since $J_{-n}(x) = (-1)^n J_n(x)$. Using (4) and substituting (7), we get

$$\begin{aligned} \mathcal{E}(|k|) &= \frac{\lambda \mathbb{E}(a^2) \zeta^4}{8\pi^2 c \Gamma_{B/\zeta}(\theta)} \int_0^{B/\zeta} e^{-b} b^{\theta+3} db \int_0^1 d|z| \int_0^{2\pi} d\psi \\ &\cdot \int_0^1 d|x| \int_0^{2\pi} d\varphi m(|z|) m(|x|) |z| |x| \frac{\cos(\psi - \varphi)}{|x|^{2\gamma} + |z|^{2\gamma}} \\ &\cdot \sum_{n=0}^{\infty} J_n(\zeta b |k| |z|) \left[\mathbf{i}^n e^{in(\psi - \alpha)} + (-1)^n \mathbf{i}^{-n} e^{-in(\psi - \alpha)} \right] \\ &\cdot \sum_{m=0}^{\infty} J_m(\zeta b |k| |x|) \left[\mathbf{i}^m e^{im(\pi - (\varphi - \alpha))} \right. \\ &\quad \left. + (-1)^m \mathbf{i}^{-m} e^{-im(\pi - (\varphi - \alpha))} \right]. \end{aligned}$$

After algebraic computations and in view of trigonometric properties, the above expression is simplified due to orthogonality of sine and cosine functions. Only the term corresponding to $m = 1, n = 1$ remain as

$$\begin{aligned} \mathcal{E}(|k|) &= \frac{4\pi^2 \lambda \mathbb{E}(a^2) \zeta^4}{c \Gamma_{B/\zeta}(\theta)} \int_0^{B/\zeta} e^{-b} b^{\theta+3} db \\ &\cdot \int_0^1 m(|z|) |z| J_1(\zeta b |k| |z|) d|z| \\ &\cdot \int_0^1 m(|x|) |x| \frac{J_1(\zeta b |k| |x|)}{|x|^{2\gamma} + |z|^{2\gamma}} d|x|. \end{aligned}$$

The Bessel function J_1 has the following asymptotic form as $|k| \rightarrow \infty$ [1]

$$\begin{aligned} J_1(|k|) &\approx \frac{1}{\sqrt{2\pi|k|}} \left[\exp\left(ik - \frac{1}{2}\pi - \frac{1}{4}\pi\right) \right. \\ &\quad \left. + \exp\left(-ik - \frac{1}{2}\pi - \frac{1}{4}\pi\right) \right]. \end{aligned} \tag{8}$$

Using (8), we compute the product of Bessel functions as

$$\begin{aligned} J_1(\zeta b |k| |z|) J_1(\zeta b |k| |x|) &\approx \frac{1}{\pi \zeta b |k| \sqrt{|x||z|}} \\ &\cdot [-\sin(\zeta b |k| (|x| + |z|)) + \cos(\zeta b |k| (|x| - |z|))]. \end{aligned}$$

Based on the above computations, we get

$$\begin{aligned} \mathcal{E}(|k|) &\propto \frac{4\pi \lambda \mathbb{E}(a^2) \zeta^3}{c |k| \Gamma_{B/\zeta}(\theta)} \int_0^{B/\zeta} e^{-b} b^{\theta+2} db \\ &\cdot \int_0^1 \int_0^1 m(|z|) m(|x|) \frac{(|x||z|)^{1/2}}{|x|^{2\gamma} + |z|^{2\gamma}} \\ &\cdot [-\sin(\zeta b |k| (|x| + |z|)) + \cos(\zeta b |k| (|x| - |z|))] d|z| d|x|. \end{aligned}$$

Making a change of variable as $\zeta b |k| = b'$, yields

$$\begin{aligned} \mathcal{E}(|k|) &\propto \frac{4\pi \lambda \mathbb{E}(a^2)}{c \zeta^\theta \Gamma_{B/\zeta}(\theta) |k|^{\theta+4}} \int_0^{B|k|} e^{-b/(|k|\zeta)} b^{\theta+2} db \\ &\cdot \int_0^1 \int_0^1 m(|z|) m(|x|) \frac{(|x||z|)^{1/2}}{|x|^{2\gamma} + |z|^{2\gamma}} \\ &\cdot (-\sin(b(|x| + |z|)) + \cos(b(|x| - |z|))) d|z| d|x|. \end{aligned}$$

After rearrangement, we have

$$\mathcal{E}(|k|) \propto \frac{4\pi \lambda \mathbb{E}(a^2) |k|^{-\theta-4}}{c \zeta^\theta \Gamma_{B/\zeta}(\theta)} \int_0^{B|k|} e^{-b/(|k|\zeta)} b^{\theta+2} f(b) db$$

where

$$\begin{aligned} f(b) &= \int_0^1 \int_0^1 m(|z|) m(|x|) \frac{(|x||z|)^{1/2}}{|x|^{2\gamma} + |z|^{2\gamma}} \\ &\quad (-\sin(b(|x| + |z|)) + \cos(b(|x| - |z|))) d|z| d|x|. \end{aligned} \tag{9}$$

The Maclaurin series of exponential function yields

$$\begin{aligned} \mathcal{E}(|k|) &\propto \frac{4\pi \lambda \mathbb{E}(a^2) |k|^{-\theta-4}}{c \zeta^\theta \Gamma_{B/\zeta}(\theta)} \int_0^{B|k|} \sum_{n=0}^{\infty} \frac{(-b/(|k|\zeta))^n}{n!} b^{\theta+2} f(b) db \\ &= \frac{4\pi \lambda \mathbb{E}(a^2) |k|^{-\theta-4}}{c \zeta^\theta \Gamma_{B/\zeta}(\theta)} \sum_{n=0}^{\infty} \frac{(-1)^n}{n! |k|^n \zeta^n} \int_0^{B|k|} b^{n+\theta+2} f(b) db. \end{aligned}$$

Using integration by parts, we get $\mathcal{E}(|k|)$ to be proportional to

$$\begin{aligned} &\frac{4\pi \lambda \mathbb{E}(a^2) |k|^{-\theta-4}}{c \zeta^\theta \Gamma_{B/\zeta}(\theta)} \left[\sum_{n=0}^{\infty} \frac{(-1)^n}{n! |k|^n \zeta^n} (B|k|)^{n+\theta+2} \int_0^{B|k|} f(b) db \right. \\ &- \sum_{n=0}^{\infty} \frac{(-1)^n}{n! |k|^n \zeta^n} (B|k|)^{n+\theta+1} (n+\theta+2) \int_0^{B|k|} f_1(b) db \\ &+ \sum_{n=0}^{\infty} \frac{(-1)^n}{n! |k|^n \zeta^n} (B|k|)^{n+\theta} (n+\theta+2)(n+\theta+1) \int_0^{B|k|} f_2(b) db \\ &- \sum_{n=0}^{\infty} \frac{(-1)^n}{n! |k|^n \zeta^n} (B|k|)^{n+\theta-1} (n+\theta+2)(n+\theta+1)(n+\theta) \\ &\cdot \int_0^{B|k|} f_3(b) db + \sum_{n=0}^{\infty} \frac{(-1)^n}{n! |k|^n \zeta^n} (B|k|)^{n+\theta-2} (n+\theta+2) \\ &\cdot (n+\theta+1)(n+\theta)(n+\theta-1) \int_0^{B|k|} f_4(b) db - \dots \left. \right] \end{aligned}$$

where suffixes of f denote the number of its indefinite integrations with respect to b [2, pg.109]. Rearranging gives

$$\begin{aligned} &\frac{4\pi \lambda \mathbb{E}(a^2) |k|^{-\theta-4}}{c \zeta^\theta \Gamma_{B/\zeta}(\theta)} \left[(B|k|)^{\theta+2} \sum_{n=0}^{\infty} \frac{(-1)^n}{n! \zeta^n} B^n \int_0^{B|k|} f(b) db \right. \\ &- (B|k|)^{\theta+1} \sum_{n=0}^{\infty} \frac{(-1)^n}{n! \zeta^n} B^n (\theta+n+2) \int_0^{B|k|} f_1(b) db \\ &+ (B|k|)^\theta \sum_{n=0}^{\infty} \frac{(-1)^n}{n! \zeta^n} B^n (\theta+n+2)(n+\theta+1) \int_0^{B|k|} f_2(b) db \\ &- (B|k|)^{\theta-1} \sum_{n=0}^{\infty} \frac{(-1)^n}{n! \zeta^n} B^n (\theta+n+2)(n+\theta+1)(n+\theta) \\ &\cdot \int_0^{B|k|} f_3(b) db \dots \left. \right]. \end{aligned}$$

It follows that the energy spectrum has the form

$$\mathcal{E}(|k|) \propto \frac{4\pi\lambda\mathbb{E}(a^2)}{c\zeta^\theta\Gamma_{B/\zeta}(\theta)}|k|^{-\theta-4}F(B|k|). \quad (10)$$

Since $f(b)$ given in (9) is a periodic and bounded function of b due to cosine and sine functions, the integrals involving $f(b)$ are bounded in the expansion of $F(b|k|)$ given above. We take them approximately as constants for large $|k|$ and write the spectrum as

$$\mathcal{E}(|k|) \propto C_1|k|^{-2} - C_2|k|^{-3} + C_3|k|^{-4} - C_4|k|^{-5} \dots \quad (11)$$

4 Comparison with an Empirical Energy Spectrum

In this section, we investigate the fit of the theoretical energy spectrum to the empirical spectrum obtained from real data. As for the data set, we use Eulerian observations along the Florida coast which have been obtained by using a radar capable of resolving scales of 250m in space and 20 minutes in time [41]. These measurements cover a region bounded by approximately 11km x 11km during 28 days. The data have been subsequently interpolated to a spatial resolution of 125m and temporal resolution of 15 min in [32] yielding a 91x91 grid. The Eulerian observations reveal eddies forming and decaying over time. Eddies which are between about 10 and 500 km in diameter are known in oceanography as mesoscale eddies and sometimes they are specified as 50 – 200km [16]. Considering these orders of magnitude, sub-mesoscale (<10-50 km) can be defined as small scale structures in the ocean. Therefore, Kolmogorov dissipation length scale is in the order of 10km. The inertial range is between 50 – 200km and the integral length scale can be taken to be 200km or a value up to 500km. Our data obtained from an area of 11km x 11km pertain to the dissipation range. In the data set, the mean flow speed U is about 1m/s. For computing the Reynolds number Re , the characteristic length scale can be taken as $L \approx 10^3$ m since the radius of the sub-mesoscale eddies in the data set is in the order of 1km. As a result, we have $Re = UL/\nu \approx 10^9$ where ν is kinematic viscosity and its typical value in ocean is $\nu = O(10^{-6})$ [12].

The solenoidal part of the interpolated data set has been filtered and Çınlar velocity field is fitted as a model in [9]. In particular, the eddy radius distribution is found to be skewed to the right as in a Gamma distribution. However, the highest radius is constrained to 5km in the estimation procedure in order to stay approximately in the spatial domain of the observations. More recently, correlation analysis is performed using the same data set in [11] where the empirical energy spectrum has been computed. This spectrum is itself a high frequency spectrum, relative to LES scales where a single grid corresponds to the whole observation area of the available data.

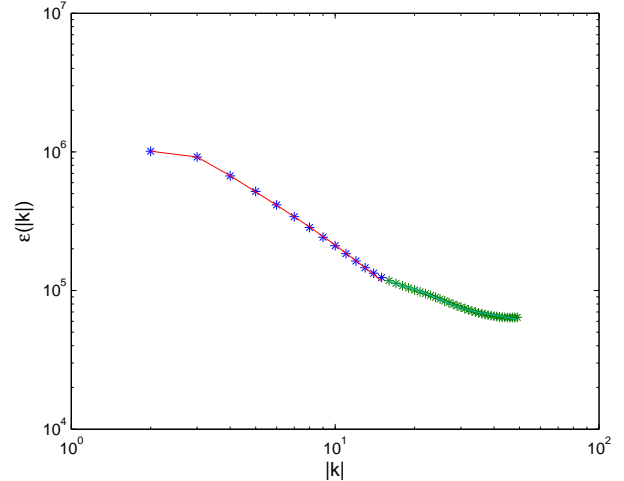


Fig. 1: Energy spectrum of first 14 days marked with * and estimated spectrum shown as solid lines, in two pieces of the wavenumber range

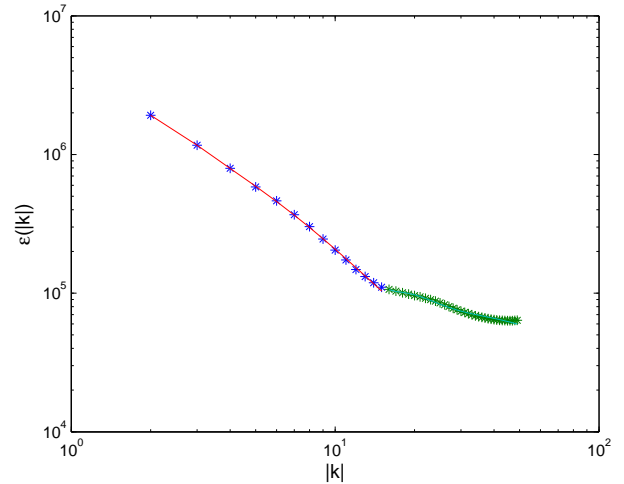


Fig. 2: Energy spectrum of last 14 days marked with * and estimated spectrum shown as solid lines, in two pieces of the wavenumber range

The energy spectrum has been obtained by a fast Fourier transform of the Eulerian data for the first and second 14-day periods [11]. Since these two parts are found to have different statistical properties in [9], they are analyzed separately. The least squares curve fitting function of MATLAB is employed for fitting (11) to the empirical energy spectrum. A good match is obtained when the range of the wave numbers k are considered in two pieces. The fitted functions as well as empirical

energy spectrum are plotted in Figures 1 and 2 for the first and second 14 day periods, respectively. The cutoff B is taken as 5km, which is about half the length of the observation domain 11kmx11km [9]. The residual norm as reported by least squares function of MATLAB is given in Table 1 for various number of terms used in the expansion of $F(b|k)$. The residual norm is defined as $\sum_{i=1}^n (y(|k|_i) - y_i)^2$ where $y_i, i = 1, \dots, n$ are the observed values of the empirical spectrum, and $y(|k|_i)$ is the predicted spectrum at wavenumber $|k|_i$. In view of Table 1 results, seven terms are used from expansion (11). Note that the residual norm is large in magnitude as the spectrum values are in the 10^5 to 10^6 range. It follows that the relative error would be in the magnitude of 10^{-1} to 10^{-2} .

Table 1: Residual norms as a function of number of terms used in the expansion of $F(b|k)$

No. of terms	First 14 days		Last 14 days	
	lower k	higher k	lower k	higher k
5	$3.55 \cdot 10^8$	$3.46 \cdot 10^8$	$2.40 \cdot 10^8$	$3.97 \cdot 10^8$
6	$1.03 \cdot 10^8$	$7.0 \cdot 10^7$	$2.41 \cdot 10^8$	$2.08 \cdot 10^8$
7	$3.13 \cdot 10^7$	$4.26 \cdot 10^7$	$2.09 \cdot 10^8$	$4.12 \cdot 10^8$
8	$1.05 \cdot 10^{10}$	$2.46 \cdot 10^7$	$6.39 \cdot 10^8$	$3.51 \cdot 10^8$
9	$7.07 \cdot 10^9$	$1.09 \cdot 10^7$	$9.97 \cdot 10^9$	$1.67 \cdot 10^8$

The function (11) that is fit to empirical spectrum is not informative for θ and ζ . The parameters of the distribution (5) can be estimated from the radius data directly. The histogram of eddy radius data was found to be right skewed with a peak at 5km in [9, Fig.6] since the estimation was performed with this cutoff. The peak at 5km can be interpreted as the unobserved larger eddies affecting the subgrid scales. Therefore, a truncated Gamma distribution is well indicated by real HF radar data for eddy radius. The eddy radius histogram after truncation of the peak at 5km in [9, Fig.6] is shown together with a right-truncated Gamma density fit in Figure 3. For the fitted density, the parameters are estimated as $\theta = 2.76$ and $\zeta = 1.64$ using maximum likelihood estimation. We have formed and solved the likelihood equations with fsolve function of MATLAB. In Figure (3), the density fit is better for the smaller radii which form the dissipation range. A mixture distribution where a both left and right-truncated Gamma distribution for $b > 2$ km could fit better to the right hand tail of the histogram. In fact, this type of two-piece fit would be consistent with the estimation of the spectrum in two pieces in Figures 1 and 2. Since the smaller scales are aimed, the estimate $\theta = 2.76$ is valid for the dissipation range. This implies $\mathcal{E}(|k|) \propto C|k|^{-6.76}F(B|k)$ from (10). It is comparable to α value being about -6 in (3). However, $F(B|k)$ remains implicit and might involve powers of $|k|$. We can compare the coefficients of the

function in (11), which is fit to the empirical spectrum, with their numerically evaluated counterparts in (10). We use the estimated values for θ, ζ , given above, and those of λ, c , and the second moment of a given in [9] together with $B = 5$ km. The results are given in Table

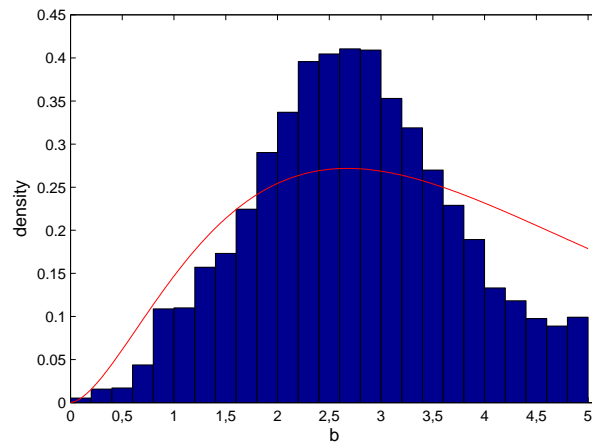


Fig. 3: Right-truncated Gamma density fit to the density histogram of eddy radius from HF radar data after truncation of 5km and above

Comparison of our results with the widely used spectrum (3) would be of interest. Since $n = 2$ is suggested for dissipation scales, we fit only α and the scale parameter β in (3). This form covers Lundgren vortex (2) with $\alpha = -5/3$. The results for the first and second half of the observation period are given in figures 4 and 5, respectively, where the estimated power α for the higher frequencies are -1.11 and -0.68 . Although the fit is somewhat less satisfactory for lower $|k|$ in Figure 4, it is good for higher wavenumbers, which are of interest, in both figures. Therefore, model (3) could be used as well for the spectrum obtained from our data.

Table 2: Comparison of the coefficients C_1 and C_2

	First 14 days		Last 14 days	
	Eq (10)	Numerical fit	Eq (10)	Numerical fit
C_1	$7.12 \cdot 10^8$	$7.94 \cdot 10^8$	$1.71 \cdot 10^9$	$6.26 \cdot 10^8$
C_2	$6.30 \cdot 10^{11}$	$6.15 \cdot 10^{10}$	$7.56 \cdot 10^{11}$	$4.23 \cdot 10^{10}$

Using MATLAB, the first two coefficients C_1 and C_2 in (10) are computed and compared with the values obtained from the numerical fit of (11) for two different periods, and lower and higher k within these periods. The results are given in Table 2 for only higher wave numbers k since

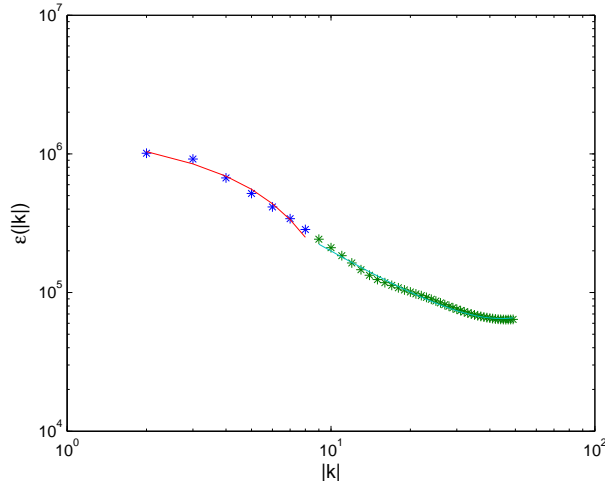


Fig. 4: Energy spectrum of first 14 days marked with * and estimated spectrum from Equation (3) shown as solid lines

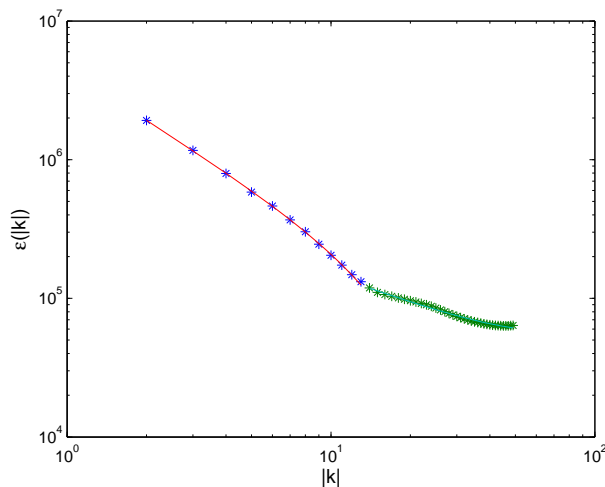


Fig. 5: Energy spectrum of last 14 days marked with * and estimated spectrum from Equation (3) shown as solid lines

the values from computation and function fit are closer in this case as consistent with the approximation being for large k . The parameter values in (10) are taken from [9] with $m(r) = (1 - \cos 2\pi r)/2$ as in [6].

5 Conclusions and Outlook

In this paper, we have derived the energy spectrum of generalized Çinlar velocity field which was shown to represent the Eulerian velocity well in the subscales and

put forward as a candidate of a subgrid model for LES in [9]. We have shown that the velocity field, which is based on rotational vortex structures, can capture the second order properties of the subgrid scale with its energy spectrum. It represents the empirical spectrum obtained from real data well and is comparable to the widely used form of energy spectrum for small scales.

We use a right-truncated Gamma distribution to find the form of the spectrum. For large $|k|$, it has the form

$$\mathcal{E}(|k|) \sim |k|^{-\theta-4} F(B|k|).$$

Although our study started with the motivation that $F(b|k|)$ could be a mixture of power and exponential functions as in the widely used form $(|k|\eta)^\alpha \exp(-\beta(|k|\eta)^n)$ of the spectrum, we have found an expansion for $F(b|k|)$, which remains implicit and must be evaluated numerically. A good match is obtained for two parts of the range of the wave numbers k . Both parts are in the subgrid scale for LES, while the higher wavenumbers represent the dissipation range. The parameter θ is estimated directly from the radius data. By fitting a truncated Gamma density, we have found the shape parameter θ to be 2.76 by maximum likelihood estimation. The widely used form of the spectrum in the literature also fits quite well to the empirical spectrum even when $n = 2$ is fixed as generally accepted.

Our results imply that a right-truncated Gamma distribution is plausible for the eddy radius. Since the spectrum does not have an inertial range, the larger eddies at supergrid scales may have a different distribution. A Pareto distribution was used in [10] to replicate $-5/3$ scaling.

Lundgren vortex [31] is a stretched spiral vortex and has been successfully used as a subgrid model for LES [35]. Çinlar velocity field being composed of randomized rotational vortices is a more complete description of the subgrid dynamics. It is a stochastic process which captures eddy arrival and decay in contrast to the static randomness of the parameters of the stretched vortex. In future work, we aim to take advantage of these features for devising a comprehensive subgrid scale model in view of the prior study [35]. From a statistical point of view, the covariance of the subgrid velocity with the resolved velocity in each step of LES can be estimated to represent the subgrid stress. We will pursue this idea to develop a numerical algorithm based on the subgrid fluctuations modeled by our velocity field.

Acknowledgement

This work was supported by The Scientific and Technological Research Council of Turkey (TUBITAK) Project No. 112T761.

The authors would like to thank the anonymous referees for their constructive comments. They also benefited from valuable discussions with Prof. Serdar Çelebi of ITU.

Appendix

Characteristic function is defined by $\varphi_u(\kappa) = \mathbb{E}(e^{i\kappa u})$ where u is the velocity field. The characteristic function of velocity increments is computed as follows

$$\begin{aligned} \varphi_{\delta u_{\parallel}(x,r)}(\kappa) &= \mathbb{E} \left[\exp i\kappa \int_{-\infty}^t \int_Q N(ds, dq) e^{-c(t-s)} \right. \\ &\quad \cdot \left. \sum_{j=1}^2 \frac{r_j}{|r|} (\mathbf{v}_q^j(x+r) - \mathbf{v}_q^j(x)) \right] \\ &= \exp \lambda \int_{-\infty}^t \int_Q ds dz \alpha(da) \beta(db) e^{-c(t-s)} \\ &\quad \cdot \left[\exp i\kappa \sum_{j=1}^2 \frac{r_j}{|r|} (\mathbf{v}_q^j(x+r) - \mathbf{v}_q^j(x)) - 1 \right] \\ &= \exp \lambda \int_{-\infty}^t ds e^{-c(t-s)} \int_Q dz \alpha(da) \beta(db) \\ &\quad \cdot \left[\exp a i \kappa \sum_{j=1}^2 \frac{r_j}{|r|} \left[\mathbf{v}_j \left(\frac{x+r-z}{b} \right) \right. \right. \\ &\quad \quad \left. \left. - \mathbf{v}_j \left(\frac{x-z}{b} \right) \right] - 1 \right]. \end{aligned}$$

Note that $\delta u_{\parallel}(x,r) = \delta u_{\parallel}(0,r)$ by homogeneity. If we rename the following functions for simplicity,

$$h(\kappa) = a i \kappa \sum_{j=1}^2 \frac{r_j}{|r|} \left[\mathbf{v}_j \left(\frac{x+r-z}{b} \right) - \mathbf{v}_j \left(\frac{x-z}{b} \right) \right]$$

$$g(\kappa) = \frac{\lambda}{c} \int_Q dz \alpha(da) \beta(db) \left[e^{h(\kappa)} - 1 \right]$$

the characteristic function of velocity increment can be written as $\varphi_{\delta u_{\parallel}}(\kappa) = e^{g(\kappa)}$. Third order derivative should be taken for skewness. The first derivative of characteristic function is

$$\frac{d\varphi_{\delta u_{\parallel}}(\kappa)}{d\kappa} = e^{g(\kappa)} g'(\kappa)$$

where $g'(\kappa) = \frac{\lambda}{c} \int_Q dz \alpha(da) \beta(db) e^{h(\kappa)} h'(\kappa)$ and $h'(\kappa) = a i \sum_{j=1}^2 \frac{r_j}{|r|} (\mathbf{v}_j(\frac{x+r-z}{b}) - \mathbf{v}_j(\frac{x-z}{b}))$. The second derivative of characteristic function is

$$\frac{d^2\varphi_{\delta u_{\parallel}}(\kappa)}{d\kappa^2} = e^{g(\kappa)} [(g'(\kappa))^2 + g''(\kappa)]$$

where $g''(\kappa) = \frac{\lambda}{c} \int_Q dz \alpha(da) \beta(db) e^{h(\kappa)} [(h'(\kappa))^2 + h''(\kappa)]$ and $h''(\kappa) = 0$. Finally, the third derivative of characteristic function is

$$\frac{d^3\varphi_{\delta u_{\parallel}}(\kappa)}{d\kappa^3} = e^{g(\kappa)} [(g'(\kappa))^3 + 3g'(\kappa)g''(\kappa) + g'''(\kappa)]$$

where $g'''(\kappa) = \frac{\lambda}{c} \int_Q dz \alpha(da) \beta(db) e^{h(\kappa)} [(h'(\kappa))^3]$.

For $\kappa = 0$

$$\begin{aligned} \varphi_{\delta u_{\parallel}}^{(3)}(0) &= \left[\frac{\lambda}{c} \int_Q dz \alpha(da) \beta(db) a i \right. \\ &\quad \cdot \left. \sum_{j=1}^2 \frac{r_j}{|r|} \left(\mathbf{v}_j \left(\frac{x+r-z}{b} \right) - \mathbf{v}_j \left(\frac{x-z}{b} \right) \right) \right]^3 \\ &\quad + 3 \frac{\lambda^2}{c^2} \int_Q dz \alpha(da) \beta(db) a i \\ &\quad \cdot \sum_{j=1}^2 \frac{r_j}{|r|} \left(\mathbf{v}_j \left(\frac{x+r-z}{b} \right) - \mathbf{v}_j \left(\frac{x-z}{b} \right) \right) \\ &\quad \cdot \int_Q dz \alpha(da) \beta(db) \\ &\quad \cdot \left[a i \sum_{j=1}^2 \frac{r_j}{|r|} \left(\mathbf{v}_j \left(\frac{x+r-z}{b} \right) - \mathbf{v}_j \left(\frac{x-z}{b} \right) \right) \right]^2 \\ &\quad + \frac{\lambda}{c} \int_Q dz \alpha(da) \beta(db) \left[a i \sum_{j=1}^2 \frac{r_j}{|r|} \left(\mathbf{v}_j \left(\frac{x+r-z}{b} \right) \right. \right. \\ &\quad \quad \left. \left. - \mathbf{v}_j \left(\frac{x-z}{b} \right) \right) \right]^3. \end{aligned}$$

After rearrangement, we have

$$\begin{aligned} \varphi_{\delta u_{\parallel}}^{(3)}(0) &= -\frac{\lambda^3}{c^3} i \mathbb{E}(a)^3 \left[\int_{\mathbb{R}^2} \int_{\mathbb{R}_+} dz \beta(db) \right. \\ &\quad \cdot \left. \sum_{j=1}^2 \frac{r_j}{|r|} \left(\mathbf{v}_j \left(\frac{x+r-z}{b} \right) - \mathbf{v}_j \left(\frac{x-z}{b} \right) \right) \right]^3 \\ &\quad - 3 \frac{\lambda^2}{c^2} i \mathbb{E}(a) \mathbb{E}(a^2) \int_{\mathbb{R}^2} \int_{\mathbb{R}_+} dz \beta(db) \\ &\quad \cdot \sum_{j=1}^2 \frac{r_j}{|r|} \left(\mathbf{v}_j \left(\frac{x+r-z}{b} \right) - \mathbf{v}_j \left(\frac{x-z}{b} \right) \right) \\ &\quad \cdot \int_{\mathbb{R}^2} \int_{\mathbb{R}_+} dz \beta(db) \left[\sum_{j=1}^2 \frac{r_j}{|r|} \left(\mathbf{v}_j \left(\frac{x+r-z}{b} \right) \right. \right. \\ &\quad \quad \left. \left. - \mathbf{v}_j \left(\frac{x-z}{b} \right) \right) \right]^2 \\ &\quad - \frac{\lambda}{c} i \mathbb{E}(a^3) \int_{\mathbb{R}^2} \int_{\mathbb{R}_+} dz \beta(db) \left[\sum_{j=1}^2 \frac{r_j}{|r|} \left(\mathbf{v}_j \left(\frac{x+r-z}{b} \right) \right. \right. \\ &\quad \quad \left. \left. - \mathbf{v}_j \left(\frac{x-z}{b} \right) \right) \right]^3. \end{aligned}$$

Due to isotropy property of velocity field, first and second summed equal to zero. Hence we obtain

$$\varphi_{\delta u_{\parallel}}^{(3)}(0) = \frac{\lambda}{c} \mathbf{i} \mathbb{E}(a^3) \int_{\mathbb{R}^2} \int_{\mathbb{R}_+} dz \beta(db) \cdot \left[\sum_{j=1}^2 \frac{r_j}{|r|} \left(v_j \left(\frac{x+r-z}{b} \right) - v_j \left(\frac{x-z}{b} \right) \right) \right]^3.$$

Using the property $\mathbb{E}(u^3) = (-\mathbf{i}^3) \varphi_{\delta u_{\parallel}}^{(3)}(0)$

$$\mathbb{E}(\delta u_{\parallel}^3) = \frac{\lambda}{c} \mathbb{E}(a^3) \int_{\mathbb{R}^2} \int_{\mathbb{R}_+} dz \beta(db) \cdot \left[\sum_{j=1}^2 \frac{r_j}{|r|} \left(v_j \left(\frac{x+r-z}{b} \right) - v_j \left(\frac{x-z}{b} \right) \right) \right]^3.$$

Using truncated Gamma distribution for b

$$\mathbb{E}(\delta u_{\parallel}^3) = \frac{\lambda}{c} \mathbb{E}(a^3) \int_{\mathbb{R}^2} \int_0^B dz db \frac{b^{\theta-1} e^{-b/\zeta}}{\Gamma_{B/\zeta}(\theta) \zeta^{\theta}} \cdot \left[\sum_{j=1}^2 \frac{r_j}{|r|} \left(v_j \left(\frac{x+r-z}{b} \right) - v_j \left(\frac{x-z}{b} \right) \right) \right]^3.$$

Making a change of variable as $z' = x - z$, yields

$$\mathbb{E}(\delta u_{\parallel}^3) = \frac{\lambda \mathbb{E}(a^3)}{c \Gamma_{B/\zeta}(\theta) \zeta^{\theta}} \int_{\mathbb{R}^2} \int_0^B dz db b^{\theta-1} e^{-b/\zeta} \cdot \left[\sum_{j=1}^2 \frac{r_j}{|r|} \left(v_j \left(\frac{z+r}{b} \right) - v_j \left(\frac{z}{b} \right) \right) \right]^3.$$

Using the specific equations for \mathbf{v} given in the text

$$\begin{aligned} \mathbb{E}(\delta u_{\parallel}^3) &= \frac{\lambda \mathbb{E}(a^3)}{c \Gamma_{B/\zeta}(\theta) \zeta^{\theta}} \int_{\mathbb{R}^2} \int_0^B dz db b^{\theta-1} e^{-b/\zeta} \quad (12) \\ &\cdot \left[\frac{r_1}{|r|} \left(\frac{-z_2 - r_2}{|z+r|} m \left(\frac{|z+r|}{b} \right) + \left(\frac{z_2}{|z|} m \left(\frac{|z|}{b} \right) \right) \right) \right. \\ &+ \left. \frac{r_2}{|r|} \left(\frac{z_1 + r_1}{|z+r|} m \left(\frac{|z+r|}{b} \right) - \frac{z_1}{|z|} m \left(\frac{|z|}{b} \right) \right) \right]^3 \\ &= \frac{\lambda \mathbb{E}(a^3)}{c \Gamma_{B/\zeta}(\theta) \zeta^{\theta}} \int_{\mathbb{R}^2} \int_0^B dz db b^{\theta-1} e^{-b/\zeta} \\ &\cdot \left(\frac{z_1 r_2 - z_2 r_1}{|r|} \right)^3 \left(\frac{m(|z+r|/b)}{|z+r|} - \frac{m(|z|/b)}{|z|} \right)^3. \end{aligned}$$

We have evaluated the integral in (12) numerically for various values of $|r|$ and found positive values as shown in Figure 6. As a result, the sign of (12) is controlled by the third moment of a . Note that the integral is constant for sufficiently large values of $|r|$ since m has compact support, and that it is sufficient to consider only $|r|$ since the velocity field is isotropic.

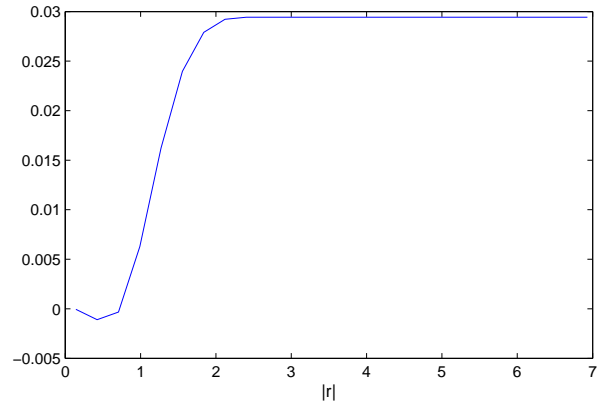


Fig. 6: The value of the integral in (12) for various values of $|r|$.

References

- [1] M. Abramowitz, I. Stegun, Handbook of Mathematical Functions with Formulas, Graphs, and Mathematical Tables. Dover Publications (1964).
- [2] N.P. Bali, "Integral Calculus", Laxmi Publications (2008).
- [3] J. Bardina, J.H. Ferziger, W.C. Reynolds, Improved subgrid scale models for large eddy simulation. AIAA Pap. 80 1357 (1980).
- [4] J.M. Burgers, A mathematical model illustrating the theory of turbulence. Adv. Appl. Mech. **1**:171-199 (1948).
- [5] J. Bardina, J.H. Ferziger, W.C. Reynolds, Improved turbulence models based on LES of homogeneous incompressible turbulent flows. Department of Mechanical Engineering, Report No. TF-19, Stanford (1984).
- [6] M. Çağlar, Simulation of homogeneous and incompressible Çınlar flows, Appl. Math. Modelling **24**: 297-314 (2000).
- [7] M. Çağlar, E. Çınlar, Lyapunov Exponents of Poisson Shot-Noise Velocity Fields. Stochastic Processes and their Applications **94**: 29-49 (2001).
- [8] M. Çağlar, Dispersion of mass by two-dimensional homogeneous and incompressible Çınlar flows. Appl. Math. Modelling, **27**: 997-1011 (2003).
- [9] M. Çağlar, L. Piterbarg, T. Ozgokmen, Parameterization of Submeso-Scale Eddy-Rich Flows using a Stochastic Velocity Model. Journal of Atmospheric and Oceanic Technology **23**:1745-1758 (2006).
- [10] M. Çağlar, Velocity Fields with Power-Law Spectra for Modeling Turbulent Flows. Applied Mathematical Modelling **31**:1934-1946 (2007).
- [11] M. Çağlar, T. Bilal, L. Piterbarg, Lagrangian Prediction and Correlation Analysis with Eulerian Data. Turkish J. Earth Sciences **20**: 343-358.
- [12] T.M. Chin, T. Ozgokmen, A.J. Mariano, Empirical and stochastic formulations of western boundary conditions. Ocean Modelling 2007; **17**:219-238 (2011).
- [13] D. Chung, D.I. Pullin, Direct numerical simulation and large-eddy simulation of stationary buoyancy-driven turbulence. J. Fluid Mech. **643**:279-308 (2012).
- [14] E. Çınlar, On a Random Velocity Field. Princeton University (1993).

- [15] E. Çınlar, Isotropic Velocity Fields of Poisson Shot Noise Type. Princeton University (1994).
- [16] A. Colling, Ocean Circulation. Butterworth-Heinemann (2001).
- [17] S. Corrsin, Turbulent dissipation fluctuations. Phys. Fluids **5**:1301–1302 (1962).
- [18] J. Deardorff, A numerical study of three-dimensional turbulent channel flow at large Reynolds numbers. Journal of Fluid Mechanics **41**: 453–480 (1970).
- [19] J.A. Domaradzki, E.M. Saiki, A Subgrid-Scale Model Based on the Estimation of Unresolved Scales of Turbulence. Phys. Fluids **9**:2148–2164 (1997).
- [20] U. Frisch, Turbulence: The Legacy of A.N. Kolmogorov. Cambridge University press, Cambridge (1995).
- [21] J.E. Gentle, Random Number Generation and Monte Carlo Methods. Springer (2003).
- [22] M. Germano, U. Piomelli, P. Moin, W. Cabot, A dynamic subgrid-scale eddy viscosity model. Physics of Fluids A **3**:1760–1765 (1991).
- [23] S. Kida, Y. Murakami, Kolmogorov similarity in freely decaying turbulence. Phys. Fluids **30**, 2030–2039 (1987).
- [24] A.N. Kolmogorov, The local structure of turbulence in incompressible viscous fluid for very high Reynolds numbers. Dokl. Akad. Nauk SSSR **30**: 301-305 (1941).
- [25] R.H. Kraichnan, The structure of isotropic turbulence at very high Reynolds numbers. J. Fluid Mech. **5**, 497–543 (1959).
- [26] R.H. Kraichnan, Diffusion by a random velocity field. Physics of Fluids **13**:22–31 (1970).
- [27] A. Leonard, Energy cascade in large-eddy simulations of turbulent fluid flows. Advances in Geophysics A **18**:237–248 (1974).
- [28] Y. Li, Lagrangian evolution of velocity increments in rotating turbulence: The effects of rotation on non-Gaussian statistics. Physica D **239**, 1948–1957 (2010).
- [29] D.K. Lilly, On the numerical simulation of buoyant convection. Tellus **14**:148–172 (1962).
- [30] D.K. Lilly, The representation of small-scale turbulence in numerical simulations. In Proceedings of IBM scientific computing symposium on environmental sciences, IBM form no. 320-1951. White Plains, New York, 195–209 (1967).
- [31] T.S. Lundgren, Strained spiral vortex model for turbulent fine structure. Phys. Fluids **25-12**:2195–2203 (1982).
- [32] A.J. Mariano, T.M. Chin, T.M. Ozgokmen, Stochastic boundary conditions for coastal flow modeling. Geophys. Res. Letters **30**: 1457-1461 (2003).
- [33] D.O. Martinez, S. Chen, G.D. Doolen, R.H. Kraichnan, L.P. Wang and Y. Zhou, Energy spectrum in the dissipation range of fluid turbulence. J. Plasma Physics **57**:195–201 (1997).
- [34] C. Meneveau, J. Katz, Scale-invariance and turbulent models for large-eddy simulation. Annual Review of Fluid Mechanics **32**:1–32 (2000).
- [35] A. Misra, D.I. Pullin, A vortex-based subgrid stress model for large-eddy simulation, Phys. Fluids **9**:2443–2454 (1997).
- [36] E.A. Novikov, Energy spectrum of turbulent flow of an incompressible fluid. Dokl. Akad. Nauk. SSR **139**, 331 (1961).
- [37] S.A. Orszag, Fluid Dynamics. Proceedings of 1973 Les Houches Summer School of Theoretical Physics (ed. R. Balian and J. L. Peube), p. 237. Gordon and Breach, New York (1977).
- [38] L.F. Richardson, L.F. Atmospheric diffusion shown on a distance-neighbour graph. Proc. R. Soc. Lond. A **110**:709–737 (1926).
- [39] P.G. Saffman, Lectures on homogeneous turbulence. In Topics in Nonlinear Physics, N. J. Zabusky, ed., Springer Verlag, 485–614 (1968).
- [40] P. Sagaut, Large Eddy Simulation for Incompressible Flows: An Introduction. Springer, (2005).
- [41] L.K. Shay et al., VHF radar detects oceanic submesoscale vortex along Florida coast. Eos Trans. **81**:209–213 (2000).
- [42] J. Smagorinsky, General Circulation Experiments with the Primitive Equations. Monthly Weather Review **91**: 99–164 (1963).
- [43] H. Tennekes, Outline of a second-order theory of turbulent pipe flow. AIAA J. **6**:1735–1740 (1968).
- [44] A.A. Townsend, On the fine scale structure of turbulence. Proc. Roy. Soc. (London) A208, 534–542 (1951).
- [45] W.R. Wade, An introduction to analysis. Pearson, Prentice Hall (2004).
- [46] H.E. Yildirim, Poisson random velocity fields: advection-diffusion properties. Dissertation. Princeton University (1998).



Rukiye Kara obtained her M.S degrees in Mathematics from Istanbul Technical University. Currently she is a Ph.D Student in Mathematics at Mimar Sinan Fine Arts University. Her research interests are in the areas of applied mathematics and mathematical physics including the statistical

solution methods of Navier-Stokes equations and large eddy simulation.



Mine Çağlar obtained her B.S and M.S degrees in Industrial Engineering from Middle East Technical University and Bilkent University, respectively. After receiving a Ph.D degree in Statistics and Operations Research from Princeton University in 1997, she worked as a post-doctoral

research scientist in Network Design and Traffic Research Group at Bellcore during 1997-98. She is currently an associate professor in the Department of Mathematics at Koc University, which she joined in 1999. Dr. Çağlar's areas of expertise are stochastic flows, self-similar processes and stochastic modeling in telecommunication networks. She has been a principal investigator of international and national research projects. In 2012, she was the co-chair of the Local Organizing Committee as well as a member of the Program Committee for the eighth World Congress in Probability and Statistics. She is an elected member of the International Statistical Institute.